Torsional properties of bamboo-like structured Cu nanowires

<u>Haifei Zhan</u> and Yuantong Gu[*]

School of Chemistry, Physics and Mechanical Engineering,
Queensland University of Technology, Brisbane, QLD, 4001, Australia
* Corresponding author: yuantong.gu@qut.edu.au

Abstract Recently, researchers reported that nanowires (NWs) are often polycrystalline, which contain grain or twin boundaries that transect the whole NW normal to its axial direction into a bamboo like structure. In this work, large-scale molecular dynamics simulation is employed to investigate the torsional behaviours of bamboo-like structured Cu NWs. The existence of grain boundaries is found to induce a considerably large reduction to the critical angle, and the more of grain boundaries the less reduction appears, whereas, the presence of twin boundaries only results in a relatively smaller reduction to the critical angle. The introduction of grain boundaries reduces the torsional rigidity of the NW, whereas, the twin boundaries exert insignificant influence to the torsional rigidity. NWs with grain boundaries are inclined to produce a local HCP structure during loading, and the plastic deformation is usually evenly distributed along the axial axis of the NW. The plastic deformation of both perfect NW and NWs with twin boundaries is dominated by the nucleation and propagation of parallel intrinsic stacking faults. This study will enrich the current understanding of the mechanical properties of NWs, which will eventually shed lights on their applications.

Keywords   Grain Boundary, Twin Boundary, Nanowire, Torsion, Molecular Dynamics

1. Introduction

Metal and semiconductor nanowires (NWs) have been widely utilized as active components of nanoelectromechanical systems (NEMS) due to their extraordinary mechanical, electrical, optical and thermal properties, such as high frequency resonators, field effect transistors (FETs), and other devices [1]. Hence, a comprehensive understanding of the mechanical properties of NWs is increasingly required. There have been a number of experimental, theoretical and computational studies on the properties of NWs. On the experimental front, researchers have studied the mechanical behaviours of NWs under bending, tension, compression and vibration. On the theoretical and computational front, either surface-based extensions of continuum elasticity theory [2] or multi-scale computational techniques [3] has been employed to investigate the mechanical properties of NWs. Besides, molecular dynamics (MD) simulations has also being frequently adopted to explore structure-property relationship for NWs under different loading conditions [4-7].

It is noticed that most of current studies have focused on mono-crystalline NWs due to the decreased possibility of defects and flaws in nanoscale materials. However, recent experimental studies reveal that NWs also contain certain defects. For instance, metal NWs are found usually polycrystalline, containing grain boundaries (GBs) that transect the whole NW normal to its longitudinal axis into a bamboo structure [8]. Sansoz et al. [9] revealed that, twin boundaries (TBs) are ubiquitous for both synthesis and properties in nano-enhanced FCC metals. Therefore, understanding the influence from GBs or TBs to the properties of NWs is crucial to enhance/realize their applications. There have been a number of studies on the mechanical behaviours of defected

NWs either with GBs, TBs or pre-existing defects. For example, Cao et al. [10] demonstrated that, polycrystalline Cu NWs exhibit tensile deformation behaviour distinctly different from their single crystal counterparts. A serial of investigation on the twinned Cu NWs under tensile deformation has been conducted by Cao and his group members [11]. Au and other metal NWs with twin boundaries have also been extensively studied by Sansoz and his group members [12]. The influence of different pre-existing defects on the mechanical properties of metal NWs under tension [13, 14], compression [15] have also been investigated. It is noticed that majority of current studies on polycrystalline NWs have emphasized on the mechanical properties under uniaxial loading conditions, and the study of their mechanical performance under torsion is still lack in the literature. Thus, we perform a comprehensive investigation of the influence from GBs or TBs on the torsional properties of Cu NWs using large-scale MD simulations in the present work.

2. Computational details

Large-scale MD simulations were carried out on bamboo-like polycrystalline Ag NWs with square cross-section, which were constructed either with GBs or coherent TBs. In detail, the bamboo-like NW with GBs were generated according to the work by Cao et al. [10], i.e., the <100> crystalline direction is chosen as the misorientation axis, and the GBs separating individual grains are $\sum 5(310)36.9°$ symmetric high-angle tilt GBs, which has a high density of coincident atomic sites across the interface (see Fig. 1a). This structure has also been experimentally observed [16] and studied using numerical simulations [10] by previous researchers. We considered a serial of such NWs that contain different numbers of GBs with an identical size (4.34 nm×4.57 nm×46.64 nm) and constant grain boundary spacing (GBS). Specifically, GBs numbers including 0, 1, 3, 4 and 9 were considered which leads the GBS ranging from 4.57-11.43 nm (that is comparable to the experimentally investigated grain size of 5-40 nm). Similarly, for the bamboo-like NW with (111) coherent TBs, a serial of NWs that contain different numbers of TBs (i.e., 0, 1, 3, 4 and 9) and a constant twin boundary spacing (TBS) were considered, with the TBS ranging from 6.26-15.65 nm (see Fig. 1b). The size of the NW was uniformly chosen as 5.90 nm×6.13 nm×63.87 nm. We modelled Cu using the embedded-atom-method (EAM) potential developed by Foiles et al. [17]. This potential was fitted to a group of parameters, including cohesive energy, equilibrium lattice constant, bulk modulus, and others [18].

During each simulation, the NW was first created assuming bulk lattice positions, and then relaxed to a minimum energy state using the conjugate gradient algorithm, i.e. the length of the NW was allowed to decrease in response to the tensile surface stress. We then used the Nose-Hoover thermostat [19, 20] to equilibrate the NW at a constant temperature 10 K (NVT ensemble) for 400 ps at a time step of 4 fs while holding the newly obtained length of the NW fixed. Finally, a pair of constant torsional loads was applied to the two ends of the NW as schematically shown in Fig. 1a. No periodic boundary conditions were utilized at any point during the simulation process. The overall simulation methodology to study the torsional properties of the NWs is identical to that used previously for mono-crystalline Cu NWs [21]. All simulations were performed using the open-source LAMMPS code developed at Sandia National Laboratories [22]. In order to recognize the defects in NWs, the centro-symmetry parameter (CSP) [23] is utilized, which increases from

zero for perfect FCC lattice to positive values for defects and for atoms close to free surfaces.
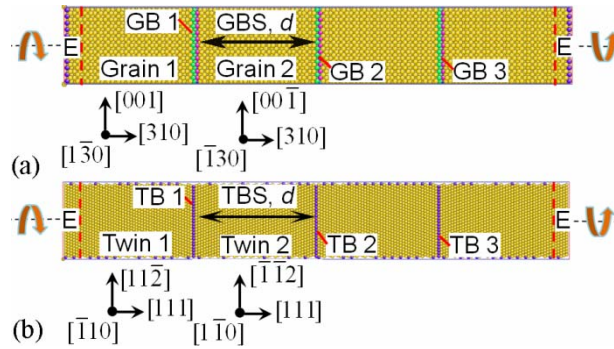

Figure 1. (a) A polycrystalline Cu NW containing three GBs with a nearly square cross-section. (b) A polycrystalline Cu NW containing three TWs with a nearly square cross-section. Both NWs were divided into three sections, including mobile region, and two rigid boundary regions 'E'.

3. Results and discussion

Following studies will focus on the impacts from GBs or TBs on the critical angle, torsional rigidity and the plastic deformation of NWs. The critical angle refers as the angle when plastic deformation or dislocations begin to emit. While the torsional rigidity (GI_p) can be obtained from the strain energy (ΔE) versus torsional angle (φ) curve through the relation of $\Delta E=(GI_p)\varphi^2/(2L)$ [21].

3.1. Polycrystalline nanowire with GBs

Mono-crystalline NW and polycrystalline NWs contain different numbers of GBs were firstly studied. Fig. 2 shows the changing trend of ΔE along with the increase of φ for these different cases. It is evident from Fig. 2 that due to the presence of GBs, the ΔE-φ curve appears a significant difference from that of the perfect NW. In detail, for the perfect NW, ΔE-φ curve exhibits a parabolic portion before yielding, after which the strain energy received an obvious reduction, and the critical angle approximates 1.627 rad. Whereas, the ΔE-φ curves for NWs with GBs show a considerably shortened parabolic portion, and this parabolic portion is apparently different from that of the perfect NW. In other words, a much smaller critical angle is observed for NWs with GBs. Particularly, ΔE-φ curves for NWs possess more than 1 GB exhibit a relatively flat fluctuation part after passing the critical angle. Selected atomic configurations are presented to investigate the deformation process of the NW.

Fig. 3 shows the atomic configurations of different NWs at different torsional angle values. Basically, for the perfect NW, the crystal structure retains its original crystal structure (see Fig. 3a1) until the torsional angle arrives 1.634 rad, which shows a relatively long elastic deformation period. After yielding, stacking faults (SFs) begin to nucleate around the centre of the NW as shown in Fig. 3a2. It is observed that, the plastic deformation has concentrated around the central area of the NW (see Fig. 3a3), which involves with the nucleation and propagation of both intrinsic and extrinsic SFs.
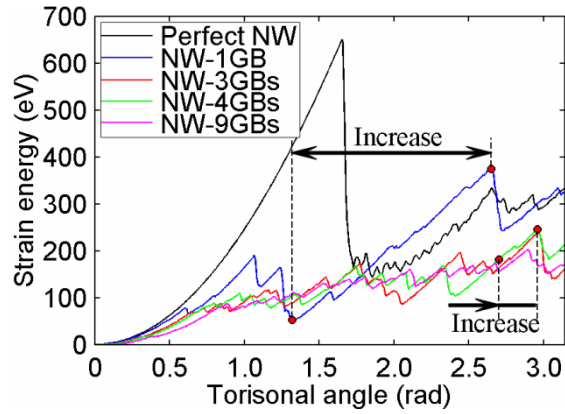
Figure 2. Strain energy versus torsional angle curves for Cu NWs with GBs.

For the NW with one GB, an extremely early yielding is observed, which only corresponds to a critical angle of 0.603 rad. The evident existence of intrinsic SF is observed at the torsional angle 0.848 rad (see Fig. 3b1), which is initiated from the location of the GB. With further loading, more SFs are generated which is associated with a sharp strain energy decrease as illustrated in Fig. 3b2. Interestingly, a local HCP structure is produced between the torsional angle around 1.319 and 2.652 rad (see Fig. 3b3), which results a considerable strain energy increase as pointed out in Fig. 2.
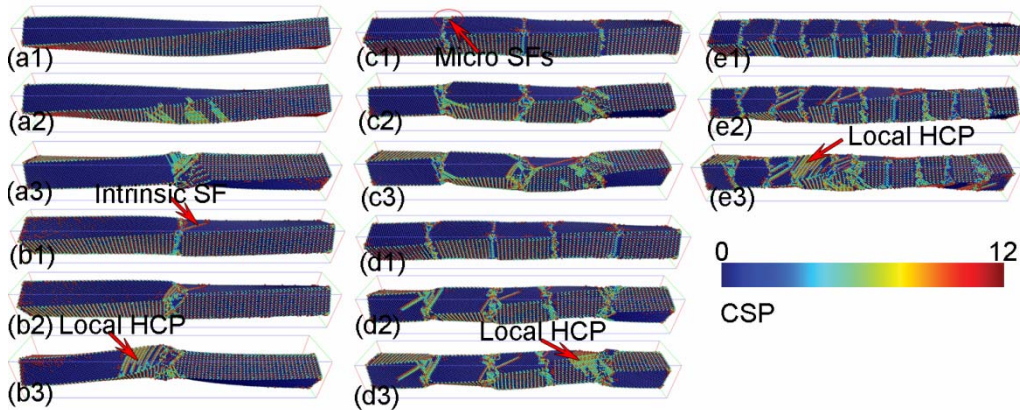

Figure 3. Atomic configurations at different torsional angles. Perfect NW: (a1) 1.634 rad, (a2) 1.665 rad, (a3) 2.482 rad; NW with one GB: (b1) 0.848 rad, (b2) 1.1 rad, (b3) 2.199 rad; NW with three GBs: (c1) 0.691 rad, (c2) 2.042 rad, (c3) 2.796 rad; NW with four GBs: (d1) 0.817 rad, (d2) 2.356 rad, (d3) 2.89 rad; NW with nine GBs: (e1) 1.759 rad, (e2) 2.733 rad, (e3) 0.911 rad.

Similar as the previous case, the NW with three GBs also exhibits a particularly early yielding (around 0.654 rad). However, in contrast to the large volume of SFs for the NW with one GB after yielding (see Fig. 3b1), only micro SFs are generated initially around the locations of GBs as shown in Fig. 3c1. Along with the increase of the torsional strain, more SFs are generated around the two outside GBs (i.e., GBs 1 and 3 in Fig. 1a) as revealed in Fig. 3c2. It is observed that, no large SFs nucleation is occurred around the middle GB (i.e., GB 2 in Fig. 1a) only until the torsional angle reaches 2.444 rad (see Fig 3c3).

For the NW with four GBs, a low critical angle around 0.798 rad is observed. After yielding, SFs

first nucleate from the two middle GBs, and their existence are found around all four GBs with further deformation, i.e., the plastic deformation is almost evenly distributed along the four GBs (see Fig. 3d2). Similar as the NW with one GB, a local HCP structure (see Fig. 3d3) is produced during the torsional angle between 2.702 and 2.959 rad, which also causes apparent strain energy resumption as highlighted Fig. 2. This structure is dissolved gradually afterwards.

The critical angle is estimated around 0.880 rad for the NW with nine GBs, after which, intrinsic SFs nucleate from the location of GBs (see Fig. 3e1). According to Fig. 3e2, the presence of SFs is found between all GBs, implying the evenly distributed plastic deformation along the NW axis. It is supposed that owing to the small GBS, further propagation of SFs is stopped by GBs, which induces a gradual increasing trend of the strain energy (refer to Fig. 2). To mention that, a local HCP structure is also generated around the middle area of the NW as illustrated in Fig. 3e3.

In short, the introduction of GBs has greatly decreased the critical angle, and led to an extremely early yielding comparing with the perfect NW. Additionally, NWs with GBs are inclined to produce a local HCP structure during loading, whose occurrence is detected for NWs with 1, 4 and 9 GBs.

3.2. Polycrystalline nanowire with TBs

We then consider polycrystalline NWs that contain different numbers of TBs. Fig. 4 illustrates the trajectory of ΔE with the increase of φ for these different cases. Different with the NWs with GBs (in Fig. 2), the elastic portion of the ΔE-φ curve for all different NWs almost overlaps with that of the perfect NW. Comparing with the critical angle of 1.703 rad, an earlier yielding is observed with the presence of TBs. Particularly, the ΔE-φ curve shows a regular reduction and resumption processes as partially shown in Fig. 4. To unveil the corresponding underlying mechanism, the atomic configurations are extensively investigated. Due to the similarity of plastic deformation, only the snapshots of the perfect NW and NWs with one, three and six TBs are presented in Fig. 5.
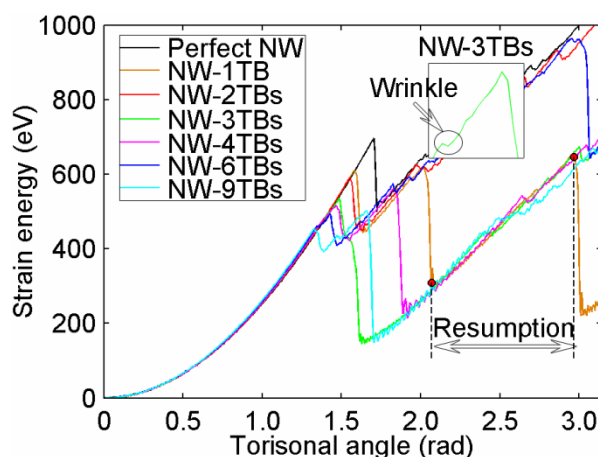

Figure 4. Strain energy versus curves for NWs with TBs.

Figure 5a1-a3 shows the atomic configurations of the perfect NW at three different torsional angles. As is seen, before yielding, the original crystal structure of the NW appears unchanged (see Fig.

5a1). Since the NW possesses a <111> axial direction, which leads to the SFs that laying on the (111) planes all perpendicular to the NW's axis. From Fig. 5a2, several parallel intrinsic SFs are observed after yielding, which initiate from the surface of the NW. With increasing loading, more parallel SFs are developed with these SFs becoming larger and larger. It is observed that, after plastic deformation, the exposure surface of the deformed area becomes {111} planes rather than the original {110} or {112} planes (see the inset of Fig. 5a3).
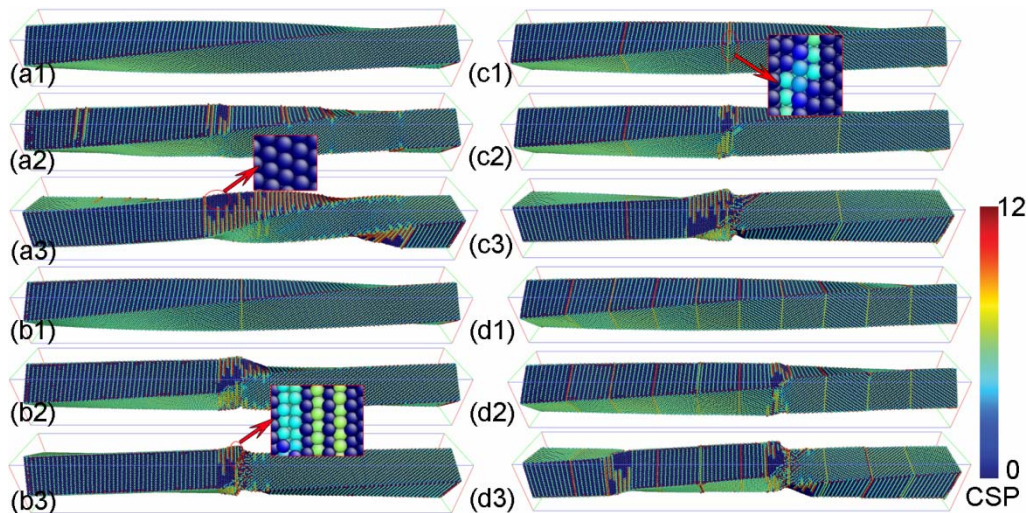

Figure 5. Atomic configurations at different torsional angles. Perfect NW: (a1) 1.696 rad, (a2) 1.728 rad, (a3) 2.827 rad; NW with one TB: (b1) 1.571 rad, (b2) 1.634 rad, (b3) 2.199 rad; NW with three TBs: (c1) 1.445 rad, (c2) 1.508 rad, (c3) 2.827 rad; NW with nine TBs: (d1) 1.382 rad, (d2) 1.319 rad, (d3) 2.827 rad.

The introduction of the TBs is found to exert obvious influence to the plastic deformation of the NW. According to Fig. 5b1, the NW with one TB also shows an intact crystal structure during elastic deformation, which however, produces less SFs than that of the perfect NW at the onset of yielding (see Fig. 5a2), and those SFs are all around the location of the TB (see Fig. 5b2). Particularly, in contrast to the pure existence of intrinsic SFs in the perfect NW, an extrinsic SF is even developed around the original twinning plane for the NW with one TB, as shown in the inset of Fig. 5b3. In addition, the deformed structure is found unchanged during several torsional angle intervals, which contributes to apparent strain energy resumptions as highlighted in Fig. 3.

NWs with three, four and six TBs show similar deformation process. Basically, for the NW with three TBs, an obvious wrinkle event is generated before the obvious strain energy decrease, as pointed out in Fig. 4, which is found to originate from the early SFs nucleation around the TB's locations (see inset of Fig. 4c1). After yielding, less SFs are usually generated around the locations of TBs comparing with the perfect NW (e.g., such as the NW with three TBs in Fig. 4c2). In particular, the plastic deformation is usually concentrated around one of the TBs, leaving the crystal structure around other TBs unchanged (see Fig. 4c3). For the NW with nine TBs, though no wrinkle event is observed, the plastic deformation is still similar as NWs with three, four and six TBs, i.e., the NW appears unchanged during the elastic deformation, and intrinsic SFs first nucleate from the locations of TBs. Specifically, most of the plastic deformation emerges in the area where SFs first nucleated. To mention that, the exposure surface of the deformed area for all defected NWs, are

uniformly found as the {111} planes.

Before concluding, we compare the critical angle among all NWs as listed in Table 1. To note that, for ΔE-φ curves that possess a wrinkle event, the torsional angle when obvious strain energy decrease occurs is taken as the critical angle. Generally, for the NW with GBs, a considerably large reduction of the critical angle is observed, e.g., for the NW with one GB, a 63.08% reduction is estimated. Furthermore, the reduction percentage is found decreased with increasing GB's number. Different from the NW with GB, the presence of TB results in a relatively smaller reduction to the critical angle, and the increase of TB's number aggravates the critical angle reduction. Additionally, from Figs. 2 and 4, the elastic portion of ΔE-φ curves appears obvious deviation and almost overlaps with that of the perfect NW for NWs with GBs and TBs, respectively. This phenomenon suggests that, the introduction of GBs will reduce the torsional rigidity, whereas, the TBs exert insignificant influence to the torsional rigidity of the NW.

Table 1. Critical angle (rad) as obtained from different tested samples.

GB/TB No.		0	1	2	3	4	6	9
NW-GB	Critical angle	1.634	0.6032	-	0.6535	0.798	-	0.8796
	Reduction (%)	-	63.08	-	60.01	51.16	-	46.17
NW-TB	Critical angle	1.696	1.577	1.552	1.483	1.464	1.426	1.382
	Reduction (%)	-	7.02	8.49	12.56	13.68	15.92	18.51

4. Conclusions

Based on the large-scale MD simulation, the torsional properties of the bamboo-like Cu NWs that contain either GBs or TBs are explored. Major conclusions are drawn as below:
- The existence of GBs induces a considerably large reduction to the critical angle, and the more of GBs the less reduction appears. On the contrary, the presence of TB results in a relatively smaller reduction to the critical angle, and the more of TBs the more severe reduction appears;
- The introduction of GBs reduces the torsional rigidity of the NW, whereas, the TBs exert insignificant influence to the torsional rigidity;
- The plastic deformation is obviously influenced by GBs. Specifically, NWs with GBs are inclined to produce a local HCP structure during loading, whose occurrence is detected for NWs with 1, 4 and 9 GBs. What's more, the plastic deformation of NWs with GBs is usually evenly distributed along the axial axis in contrast to the concentrate plastic deformation around the middle region for the perfect NW;
- A similar plastic deformation mechanism is observed for both perfect NW and NWs with TBs, i.e., dominated by the nucleation and propagation of parallel intrinsic SFs. Same as the NWs with GBs, all partial dislocations are initiated from the locations of TBs.

This study will enrich the current understanding of the mechanical properties of NWs, which will eventually shed lights on the applications of NWs.

References

[1] P. Xie, Q. Xiong, Y. Fang, Q. Qing, and C. M. Lieber, Local electrical potential detection of DNA by nanowire-nanopore sensors, *Nat. Nanotechnol.,* 7 (2011), pp. 119-125.

[2] G. Wang and X. Feng, Surface effects on buckling of nanowires under uniaxial compression, *Appl. Phys. Lett.,* 94 (2009), p. 141913.

[3] H. S. Park and P. A. Klein, Surface stress effects on the resonant properties of metal nanowires: the importance of finite deformation kinematics and the impact of the residual surface stress, *J. Mech. Phys. Solids,* 56 (2008), pp. 3144-3166.

[4] H. S. Park and J. A. Zimmerman, Modeling inelasticity and failure in gold nanowires, *Phys. Rev. B,* 72 (2005), p. 54106.

[5] H. F. Zhan and Y. T. Gu, A fundamental numerical and theoretical study for the vibrational properties of nanowires, *J. Appl. Phys.,* 111 (2012), pp. 124303-9.

[6] H. F. Zhan and Y. T. Gu, Theoretical and numerical investigation of bending properties of Cu nanowires, *Comput. Mater. Sci.,* 55 (2012), pp. 73-80.

[7] H. F. Zhan and Y. T. Gu, Modified beam theories for bending properties of nanowires considering surface/intrinsic effects and axial extension effect, *J. Appl. Phys.,* 111 (2012), p. 084305.

[8] A. Bietsch and B. Michel, Size and grain-boundary effects of a gold nanowire measured by conducting atomic force microscopy, *Appl. Phys. Lett.,* 80 (2002), pp. 3346-3348.

[9] F. Sansoz, H. Huang, and D. H. Warner, An atomistic perspective on twinning phenomena in nano-enhanced fcc metals, *JOM Journal of the Minerals, Metals and Materials Society,* 60 (2008), pp. 79-84.

[10] A. Cao, Y. Wei, and E. Ma, Grain boundary effects on plastic deformation and fracture mechanisms in Cu nanowires: Molecular dynamics simulations, *Phys. Rev. B,* 77 (2008), p. 195429.

[11] A. Cao and Y. Wei, Atomistic simulations of the mechanical behavior of fivefold twinned nanowires, *Phys. Rev. B,* 74 (2006), p. 214108.

[12] C. Deng and F. Sansoz, Fundamental differences in the plasticity of periodically twinned nanowires in Au, Ag, Al, Cu, Pb and Ni, *Acta Mater.,* 57 (2009), pp. 6090-6101.

[13] H. F. Zhan and Y. T. Gu, Atomistic exploration of deformation properties of copper nanowires with pre-existing defects, *CMES: Computer Modeling in Engineering & Sciences,* 80 (2011), pp. 23-56.

[14] H. F. Zhan, Y. T. Gu, C. Yan, X. Q. Feng, and P. Yarlagadda, Numerical exploration of plastic deformation mechanisms of copper nanowires with surface defects, *Comput. Mater. Sci.,* 50 (2011), pp. 3425-3430.

[15] H. F. Zhan and Y. T. Gu, "Molecular dynamics study of dynamic buckling properties of nanowires with defects," in *14th Asia-Pacific Vibration Conference*, HongKong, 2011.

[16] K. L. Merkle, High-resolution electron microscopy of grain boundaries, *Interface Sci.(Netherlands),* 2 (1995), pp. 311-345.

[17] S. M. Foiles, M. I. Baskes, and M. S. Daw, Embedded-atom-method functions for the fcc metals Cu, Ag, Au, Ni, Pd, Pt, and their alloys, *Phys. Rev. B,* 33 (1986), pp. 7983-7991.

[18] A. Voter, Embedded atom method potentials for seven fcc metals: Ni, Pd, Pt, Cu, Ag, Au, and Al, *Los Alamos Unclassified Technical Report LA-UR,* (1993), pp. 93-3901.

[19] W. G. Hoover, Canonical dynamics: Equilibrium phase-space distributions, *Phys. Rev. A,* 31 (1985), pp. 1695-1697.

[20] S. Nosé, A unified formulation of the constant temperature molecular dynamics methods, *J. Chem. Phys.,* 81 (1984), p. 511.

[21] H. F. Zhan, Y. T. Gu, C. Yan, and P. K. D. V. Yarlagadda, Numerical exploration of the defect's effect on mechanical properties of nanowires under torsion, *Adv. Mat. Res.,* 335 (2011), pp. 498-501.

[22] S. Plimpton, Fast parallel algorithms for short-range molecular dynamics, *J. Comput. Phys.,* 117 (1995), pp. 1-19.

[23] C. L. Kelchner, S. J. Plimpton, and J. C. Hamilton, Dislocation nucleation and defect structure during surface indentation, *Phys. Rev. B,* 58 (1998), pp. 11085-11088.